Journal of Materials Chemistry A

PAPER

View Article Online
View Journal | View Issue

Cite this: J. Mater. Chem. A, 2014, 2, 14563

Efficient adsorption/photodegradation of organic pollutants from aqueous systems using Cu_2O nanocrystals as a novel integrated photocatalytic adsorbent†

Hong-Yu Jing,‡[b] Tao Wen,‡[c] Cong-Min Fan,[a] Gui-Qi Gao,[a] Sheng-Liang Zhong[b] and An-Wu Xu*[a]

Received 15th May 2014
Accepted 2nd July 2014

DOI: 10.1039/c4ta02459a

www.rsc.org/MaterialsA

In this work, novel uniform Cu_2O nanocrystals (NCs) with a size of 4 nm were synthesized by a remarkably simple and facile route *via* a synproportionation reaction of Cu^{2+} with metal copper powder at room temperature. The obtained Cu_2O NCs as an integrated photocatalytic adsorbent (IPCA) exhibited high adsorption affinity combined with superior photocatalytic activity for the removal of various organic pollutants (humic acid (HA), Congo red (CR), methyl orange (MO) and tetracycline (TC)) in our experiments. The results show that the Langmuir isotherms were applicable to describe the adsorption processes and the adsorption kinetics followed the pseudo-second-order mode. The adsorption mechanism that is responsible for superior adsorption capacity occurs mainly *via* surface complexation as well as coagulation on the surface of Cu_2O NCs. A remarkable maximum adsorption capacity toward HA (405.5 mg g^{-1}) was achieved on Cu_2O NCs, which is higher than any currently reported adsorbents. On the basis of the batch adsorption experiments, the as-prepared Cu_2O NCs as IPCA were further applied to photodegradation experiments. More than 99.5% HA molecules could be degraded within 2 h, and the photocatalytic efficiency of Cu_2O NCs did not decrease obviously after five cycles, indicating that our Cu_2O NCs are stable IPCAs. Moreover, the Cu_2O NCs also exhibit excellent degradation efficiency for other organic pollutants (99% for CR, 90% for MO, and 75% TC, respectively). In addition, more than 94% of natural organic matter (NOM) was eliminated by Cu_2O NCs from real wastewater, which is served as drinking water in Togtoh County, Inner Mongolia, China. Therefore, obtained Cu_2O NCs can be used as a novel IPCA material for the efficient purification of NOM of contaminated ground water.

Introduction

Persistent organic pollutants in the aquatic ecosystem are a current worldwide and serious environmental issue due to their high carcinogenicity and toxicity. Some emerging environmental contaminants, such as humic substances, pharmaceuticals, dyestuffs, pesticides, and other aromatic pollutants, have aroused serious public concern because of their high solubility and persistence in water.[1,2] Humic acid (HA), as a model compound for natural organic matter (NOM), is among the humic substances formed by the breakdown of animal and vegetable matter in the environment. The presence of HA in drinking water may cause taste, colour, and odour problems. Furthermore, HA can promote microbiological regrowth in the distribution system.[3] Although HA itself is not harmful to human health, its reactions with halogen-based disinfecting agents generates a range of disinfection by-products which are associated with an increasing risk of cancer (*e.g.* bladder, colon and rectal), reproductive and developmental problems.[4] Tetracycline (TC), one of the most commonly used antibiotics in animal husbandry and fish farming, could destruct the ecosystem balance, develop resistant genes, and harm human health when it enters into aqueous environments. Azo dyes including methyl orange (MO) and Congo red (CR) are an abundant class of synthetic colored organic compounds that comprise about half of the textile dyestuffs used today. Dyes also have caused water pollution due to their toxicity. In addition, organic pollutants containing aromatic species in sources of drinking water have provided a more serious threat to human

[a]Division of Nanomaterials and Chemistry, Hefei National Laboratory for Physical Sciences at Microscale Department, University of Science and Technology of China, Hefei 230026, P.R. China. E-mail: anwuxu@ustc.edu.cn

[b]College of Chemistry and Chemical Engineering, Jiangxi Normal University, Nanchang 330022, P.R. China

[c]Institute of Plasma Physics, Chinese Academy of Sciences, Hefei 230031, P.R. China

† Electronic supplementary information (ESI) available. See DOI: 10.1039/c4ta02459a

‡ H. Y. Jing and T. Wen contributed equally to this work.

health than others. Effective removal of aqueous pollutants from the environment using new materials and techniques has always been a significant subject.[5] Various studies have focused on the efficient elimination of organic pollutants from the aquatic environment such as by electrolysis, membrane separation, coagulating sedimentation, photocatalysis, adsorption, *etc.*[6–10] Among these methods, integrated adsorption and degradation are considered to be one of the simplest and most attractive methods for toxic gas, heavy metal ions and organic pollution purification. A new material, termed as integrated photocatalytic adsorbents (IPCAs), has high adsorption affinity and photocatalytic activity for organic pollutants, such as activated carbon, silica gel, and clay-supported TiO_2.[11–13] Semiconductor-based photocatalysis has been intensively developed as an effective method for solving the current environmental problems with the utilization of solar energy, which has been considered as the ultimate solution to achieve degradation of organic pollutants completely.[14] However, the conventional powder catalysts suffer from either low efficiency in the use of visible light irradiation or the difficulty in separation from aqueous solutions after photocatalysis. To meet the rapid and efficient decomposition of organic pollutants, to design and fabricate highly efficient IPCAs in a low-cost and simple way still remains a significant challenge for organic pollutants' purification in real applications.

Cuprous oxide (Cu_2O), a p-type semiconductor with a direct band gap of about 2.17 eV, has potential applications in solar energy conversion, catalysis, lithium ion batteries, gas sensors, and electronics.[15] Cu_2O can also be used in photocatalytic degradation of organic pollutants under visible light irradiation. The lowest of the conduction band and the top of the valence band have the same parity, hence electric dipole transition between them is forbidden.[16] However, the commercial Cu_2O (CM Cu_2O) and big sized Cu_2O crystals have restricted its adsorption and photocatalytic activity. The ability to control the particle morphology is an important objective in the preparation of nanocrystals, as size and shape can significantly affect various properties.[17,18] In this paper, we report a novel route for the synthesis of Cu_2O nanocrystals (NCs) *via* a synproportionation reaction between Cu^{2+} and copper powder in aqueous solution at room temperature. The synproportionation reaction is based on the fact that two reactants have different oxidation states and combine to form an intermediate oxidation state. Recently, our group has reported that Sn^{2+} self-doped SnO_{2-x} NCs with high visible light photocatalytic activity were successfully fabricated by a synproportionation reaction of Sn^{4+} and Sn powder.[14] The obtained Cu_2O NCs have a tiny size (*ca.* 4 nm) and a large surface area. Quantum size effects for Cu_2O NCs result in positive improvement in photocatalytic activity. Evaluated by adsorption and degradation experiments of HA, MO, CR and TC, Cu_2O NCs show superior adsorption coupled with photocatalytic activity for these pollutants' removal. Notably, the excellent reusability of the Cu_2O NCs has been confirmed in the photocatalytic efficiency after 5 successive cycles, indicating that the Cu_2O NCs used as an IPCA is very stable. Moreover, about 94% natural organic matter can be removed from real groundwater by using obtained Cu_2O NCs as IPCA.

Experimental section

Cu_2O nanocrystal fabrication

For the synthesis of Cu_2O NCs, 1 mmol $CuCl_2 \cdot 2H_2O$ was dissolved in distilled water (15 mL), thereafter, metal copper powder (0.5 mmol) was added into the above solution under vigorous stirring for 6 hours. The yellow-green precipitates were collected by centrifugation, washed with distilled water for several times and dried in a vacuum oven at 60 °C overnight. In this work, the samples with different molar ratios (r) of Cu–$CuCl_2$ ($r = 1:8$, 1 : 4, 1 : 2 and 1 : 1, respectively) were also synthesized following the similar procedure. All reagents were analytical grade and used without any further purification.

Characterization of Cu_2O nanocrystals

Scanning electron microscopy (SEM) was carried out using a JEOL JSM-6330F operating at a beam energy of 15.0 kV. Transmission electron microscopy (TEM) and high resolution transmission electron microscopy (HRTEM) were performed on a JEOL-2010 microscope operating at 200 kV. X-ray powder diffraction patterns (XRD) were collected using a Rigaku/Max-3A X-ray diffractometer with Cu Kα radiation ($\lambda = 1.54178$ Å) at 40 kV and 200 mA. X-Ray photoelectron spectroscopy (XPS) was performed on a Perkin-Elmer RBD upgraded PHI-5000C ESCA system. A Shimadzu spectrophotometer (Model 2501 PC) was used to record the UV-Vis absorbance spectra in the region of 220 to 800 nm. $BaSO_4$ was used as the reflectance standard material. UV-Vis absorption spectra were acquired with the use of a Shimadzu SOLID3700 spectrophotometer. Fourier transform infrared (FTIR) spectra were recorded on a Nicolet Nexus spectrometer with samples embedded in KBr pellets. The N_2-BET (Barrett–Emmett–Teller) surface area was measured with a Micromeritics ASAP 2010 system at 77 K. The zeta potential values were measured using a ZETASIZER 3000 HSA system.

Batch adsorption measurements

The stock aqueous solutions containing 1000 mg L^{-1} of different organic pollutants (HA, CR, MO and TC) were prepared, respectively. Typically, the adsorbent abilities of the samples were evaluated by the adsorption of humic acid (HA) at room temperature using the as-prepared Cu_2O NCs and commercial Cu_2O (CM Cu_2O). To assess the organic pollutant adsorption capacities, 5 mg of Cu_2O NCs and CM Cu_2O were suspended in a 50 mL screw-capped container with different organic pollutant concentrations ranging from 5 mg L^{-1} to 200 mg L^{-1}, respectively. To clarify the pH effect, batch adsorption experiments were conducted at different pH values from 2–11, and the desired pH of the suspensions in each container was adjusted by adding small volumes of 0.01 M or 0.1 M $HClO_4$ or NaOH. For the kinetic experiments, the Cu_2O NCs dosage was maintained at 0.1 mg L^{-1} in 40 mg L^{-1} of various pollutants. After appropriate time intervals, the solid phase was separated from the solution by centrifugation at 10 000 rpm for 10 min. The concentration of different organic pollutants in the supernatant was determined by using a U-3900/3900H UV-Vis spectrophotometer (Hitachi). The pollutant adsorption percentage

over the adsorbent was calculated from the difference between the initial concentration (C_0) and equilibrium concentration (C_e) (adsorption% = $(C_0 - C_e)/C_0 \times 100\%$, and $q_e = (C_0 - C_e)/m \times V$, where q_e is the amount of pollutant adsorbed on per weight of Cu_2O NCs, V is the volume of the suspension, and m is the mass of the adsorbent). All batch adsorption experiments were carried out in the dark to avoid photocatalytic reaction.

Evaluation of photocatalytic activity

Photocatalytic activity of obtained Cu_2O NCs was tested by the photocatalytic decomposition of humic acid, Congo red, methyl orange, and tetracycline with visible light illumination after adsorption. For decomposition of HA, 5 mg of photocatalyst was dispersed in 50 mL of 40 mg L^{-1} HA aqueous solution in a reactor of double layer cooled by running water to keep the temperature unchanged. In the experiments of decomposition of MO, CR and TC, the pollutants' concentration was 10 mg L^{-1}. Prior to irradiation, the suspension was magnetically stirred in the dark for 30 min to ensure the establishment of an adsorption/desorption equilibrium between the photocatalyst and pollutants. Then the suspension was irradiated by using a Xe lamp (GX-500) combined with a UV cutoff filter ($\lambda \geq 400$ nm) under stirring. At given time intervals, about 3 mL aliquots were sampled, centrifuged with 12 000 rpm, and filtered through a 0.45 μm membrane filter to remove the remaining particles. The photo degradation of pollutants was monitored with a U-3900/3900H UV-Vis spectrophotometer (Hitachi). The organic concentration after adsorption equilibrium is regarded as the initial concentration (C_0). Additionally, the recycle experiments were also carried out for five consecutive cycles to test the durability. After each cycle, the catalyst was filtrated and washed thoroughly with ethanol for several times to remove residual impurities, and then dried at 60 °C for the next test.

Results and discussion

Characterization of Cu_2O NCs

To investigate the crystallographic structure of the as-obtained samples, the X-ray diffraction (XRD) pattern of the as-prepared sample is shown in Fig. 1. The main diffraction peaks of the XRD pattern for the obtained sample ($r = 1:2$) can be readily indexed as the cubic cuprite structure of Cu_2O (JCPDS no. 05-0667), whose calculated lattice constant $a = 4.271$ Å. No impurity phases were found for this sample. The intense and sharp diffraction peaks indicate that obtained Cu_2O NCs have high-crystallinity and a small size in spite of room temperature growth. The reaction mechanism based on a synproportionation reaction between copper and Cu^{2+} ions is shown in eqn (1):

$$Cu\ (s) + Cu^{2+}\ (aq) + H_2O\ (l) \rightarrow Cu_2O\ (s) + 2H^+\ (aq) \quad (1)$$

eqn (1) can comprise of two half reactions, eqn (2) and (3):

$$2Cu^{2+} + 2e^- + H_2O \rightarrow Cu_2O + 2H^+ \quad (2)$$

$$2Cu - 2e^- + H_2O \rightarrow Cu_2O + 2H^+ \quad (3)$$

Based on the oxidation potential and reduction potential of Cu^+ ($E^0_{Cu^{2+}/Cu_2O} = 0.1701$ V, $E^0_{Cu_2O/Cu} = -0.3557$ V *vs.* SHE), the standard Gibbs free energy ($\Delta_r G^0_m$) based on the reaction eqn (2) and (3), could be estimated to be −101.48 kJ mol^{-1}, thus, from the thermodynamics point of view, this is a spontaneous reaction at room temperature. To investigate the synthetic mechanism, a series of additional experiments with different molar ratios (r) of Cu–$CuCl_2$ ($r = 1:8$, 1 : 4, 1 : 2 and 1 : 1, respectively) were carried out following the same procedure. The XRD patterns of the samples with different Cu–$CuCl_2$ molar ratios, ranging from 1 : 8 to 1 : 1, are shown in Fig. S1.† When the Cu–$CuCl_2$ molar ratio is lower than 1 : 2, such as 1 : 4, 1 : 8, impurity phases (Cu(OH)Cl) together with Cu_2O were detected, suggesting that pure Cu_2O cannot be obtained under these conditions. While at $r = 1:1$, the diffraction peaks of partially unreacted Cu appear in the XRD pattern of this sample, indicating that not all solid Cu (metallic) can react with Cu^{2+} completely. Therefore, in this study, we chose the optimum molar ratio of Cu–$CuCl_2$ (1 : 2) to obtain pure Cu_2O NCs for adsorption and photocatalysis.

The microstructure of the Cu_2O NCs was examined by scanning electron microscopy (SEM), transmission electron microscopy (TEM) and high resolution transmission electron microscopy (HRTEM). As shown in Fig. 2a and b, obtained Cu_2O NCs have a very small particle size and a typical disordered mesostructure formed by nanoparticle aggregation. Cu_2O NCs

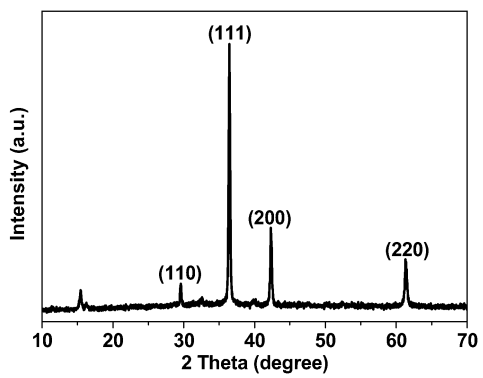

Fig. 1 XRD pattern of Cu_2O NCs at room temperature.

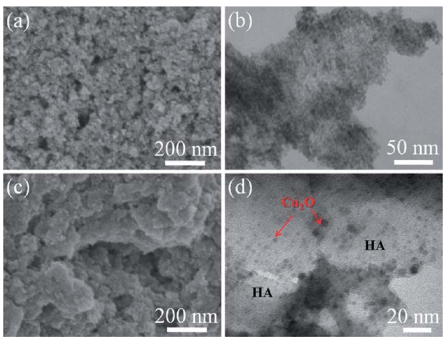

Fig. 2 SEM (a) and TEM (b) images of obtained Cu_2O NCs; SEM (c) and TEM (d) images of HA adsorbed on Cu_2O NCs.

have a uniform size and the average particle size is estimated to be around 4 nm from the TEM image. There exists a mesoporous structure formed by aggregation of nanoparticles that is beneficial for light-scattering inside their pore channels and thus improving the light harvesting capability of the obtained NCs.[19] The HRTEM image (Fig. S2a†) indicates that the lattice fringes measured with a spacing of 0.25 nm and 0.21 nm are clearly observed, corresponding to the (111) and (200) planes of Cu_2O, respectively. Energy-dispersive X-ray spectroscopy (EDS) analysis further confirms that the representative peaks corresponding to Cu and O elements exist and the Cu–O atomic ratio is about 2 : 1 (Fig. S2b†), indicating that Cu_2O NCs were successfully synthesized at room temperature.

Adsorption of organic pollutants from an aqueous environment

To investigate the adsorption performance of Cu_2O NCs, a series of systematic experiments were carried out to examine the removal of organic pollutants (HA, CR and MO). From Fig. 3a, it can be clearly seen that the adsorption rates of these three organic pollutants adsorbed on obtained Cu_2O NCs were considerably fast within the initial contact time of 30 min, and then increased slowly till the adsorption equilibrium. More than 97% (HA), 87% (MO) and 85% (CR) were removed from aqueous solution by Cu_2O NCs within 1 h. In comparison, for commercial Cu_2O, the adsorption percentages were found to be only 34% (HA), 5% (MO) and 28% (CR), indicating that our obtained Cu_2O NCs have superior adsorption capacity. The pseudo-second-order rate model ($t/q_t = 1/k_2q_e^2 + t/q_e$) was applied to simulate the experimental data in order to calculate the pseudo-second-order rate constants (k_2, g mg^{-1} min^{-1}) and the amount of pollutants adsorbed at equilibrium (q_e).[20] The kinetics of the adsorption process is shown in Fig. S3 (ESI†). The kinetic parameters of calculated and experimental q_e values, pseudo-second-order rate constants k_2, and correlation coefficient (R^2) are summarized in Table S1.† The high correlation coefficient and the agreement of calculated and experimental q_e values both suggested that the adsorption kinetics followed the pseudo-second-order model very well. Digital pictures of HA, CR, and MO adsorption on Cu_2O NCs were taken at different time intervals. As clearly noticed from Fig. S4,† HA, CR, and MO were fast adsorbed and coagulated on Cu_2O NCs in 10 min. It is noted that after adsorption, Cu_2O NCs were wrapped by humic acid, as confirmed by SEM and TEM measurements. It can be clearly seen from the SEM image of Fig. 2c that abundant agglomerates pieces with a large size were formed, and the TEM image (Fig. 2d) illustrates that Cu_2O NCs were evenly distributed on HA and wrapped by humic acid. Based on these results, HA molecules are not only adsorbed but also aggregate on the surfaces of Cu_2O NCs.

The influence of the initial solution pH on the removal of HA by Cu_2O NCs was also investigated. From Fig. S5a,† it can be seen that the adsorption percentage maintained very high (95%) in the pH range of 2.0–8.0. And then the adsorption of HA decreased dramatically from 90% to 5% when solution pH increased from 8.0 to 11.0. To further understand the effect of pH on HA adsorption, the change in the zeta potential values of Cu_2O NCs *versus* pH was measured and shown in Fig. S5b.† The pH_{pzc} (point of zero charge) value of Cu_2O NCs is ~8.2. Hence, the surface charges of Cu_2O NCs carry positive charges which are favorable for the binding of negatively charged HA anions at pH < pH_{pzc}. While at pH > pH_{pzc}, the surfaces of Cu_2O NCs are negatively charged, which makes it difficult for HA anions to adsorb on Cu_2O NCs due to the electrostatic repulsion force. Additionally, the concentration of OH^- in aqueous solution increases with increasing solution pH. These OH^- anions can also strongly compete with HA anions for binding on the surface sites of adsorbents.[21,22]

Adsorption isotherms and the possible adsorption mechanism

A maximum adsorption capacity of 405.5 mg g^{-1} was achieved on the Cu_2O NCs for HA, which exhibits superior adsorption capacity as compared with CM Cu_2O (212.3 mg g^{-1}). It is found that the as-prepared Cu_2O NCs have a BET surface area of 4.98 m^2 g^{-1}, almost over five times that of CM Cu_2O (1.04 m^2 g^{-1}). Because of the high specific surface area, the Cu_2O NCs displays superior adsorption ability of organic pollutants. Based on the above experimental results, the adsorption capacities of HA, CR, and MO on CM Cu_2O and Cu_2O NCs were investigated and are presented in Fig. 3b and S6.† Both Langmuir ($q_e = bq_{max}C_e/(1 + bC_e)$) and Freundlich ($q_e = kC_e^{1/n}$) models were applied to describe the adsorption of pollutants on the Cu_2O samples (where C_e is the equilibrium concentration of pollutants in aqueous solution (mg L^{-1}), q_e represents the amount of pollutants adsorbed on per weight of Cu_2O (mg g^{-1}); q_{max} is the maximum adsorption capacity calculated by the Langmuir equation to form a complete monolayer coverage on the surface (mg g^{-1}), b is enthalpy of sorption and should vary with temperature (L mg^{-1}), and k and $1/n$ are the Freundlich constants associated with the adsorption capacity and adsorption intensity, respectively).[23] The related parameters calculated from Langmuir and Freundlich isotherm models are shown in Table S2.† The adsorption of organic pollutants on Cu_2O NCs can be fitted very well by the Langmuir model (R^2 > 0.99), indicating that the as-prepared Cu_2O NCs have a homogeneous distribution of active sites and the adsorption sites possess equal adsorbate affinity. It is found that the maximum adsorption capacity of CR and MO adsorption on Cu_2O NCs is

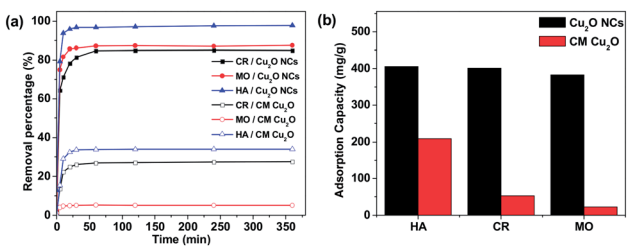

Fig. 3 (a) Adsorption isotherms of organic pollutants on Cu_2O NCs and CM Cu_2O; (b) comparison of adsorption capacity of Cu_2O NCs and CM Cu_2O for CR, MO and HA, respectively.

401.4 and 382.9 mg g^{-1}, much higher than that of CM Cu_2O, respectively. These values are remarkably larger than that of most of the reported adsorbents (Table S3†). Herein, our obtained Cu_2O NCs exhibited excellent adsorption capacity and could be used as a suitable material for the preconcentration and removal of organic pollutants.

To unravel the interaction mechanism between pollutants and Cu_2O NCs, the FTIR and XPS spectra of Cu_2O NCs before and after HA adsorption were recorded (Fig. 4). As shown in Fig. 4a, the broad band at 3450 cm^{-1} corresponds to the stretching modes of O–H groups and the bands in the range of 500–800 cm^{-1} are ascribed to Cu–O, O–Cu–O, and Cu–O–Cu lattice vibrations.[24] After HA adsorption, different functional groups are found in the FTIR spectrum of HA, *i.e.*, C=O group and COO^- at 1619 cm^{-1}, and antisymmetric stretching vibration of COO^- at 1454 cm^{-1}. The strong peaks at 2922 cm^{-1} and 2854 cm^{-1} are attributed to the vibration mode of alkane of the aliphatic series of HA. FTIR data clearly indicate that HA has been adsorbed on the surface of Cu_2O NCs. X-ray photoelectron spectroscopy was further used to analyze the surface chemical states of the HA adsorbed on Cu_2O NCs. Compared with the CM Cu_2O, the Cu 2p main peak of Cu_2O NCs occurs with a weak satellite feature and shifts to higher binding energy because of very small particle size and quantum size effect (Fig. S7†). The XPS spectrum survey is displayed in Fig. 4b. The relative intensity of the C 1s peak at 288.8 eV (O–C=O) after HA adsorption is much higher than that of the C 1s peak of pure Cu_2O NCs, suggesting that Cu_2O NCs provide binding sites to coordinate HA. In addition, the high resolution Cu 2p spectrum (Fig. 4c) shows that the Cu $2p_{3/2}$ peak at 932.7 eV is shifted to a higher binding energy after HA adsorbed on Cu_2O NCs, which results from the change in the oxidation of chemosorption, clearly demonstrating the strong interactions between Cu_2O NCs and HA molecules. The slight shift of the O 1s peak at 531.8 eV is also observed after HA adsorption (Fig. 4d), indicating the alteration of the local bonding environments.[25] From the SEM and TEM images (Fig. 2b and d), Cu_2O NCs were adsorbed and wrapped by humic acid. Thus, HA adsorption occurs mainly through surface complexation as well as coagulation on the surface of Cu_2O NCs.

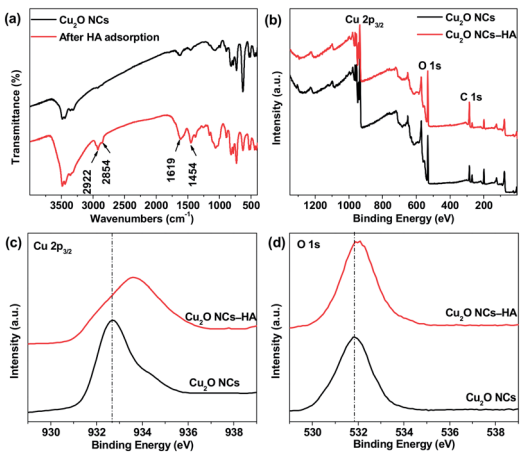

Fig. 4 FTIR spectra of Cu_2O NCs and after HA adsorption (a); XPS survey spectra of Cu_2O NCs and after HA adsorption (b); XPS spectra of Cu $2p_{3/2}$ (c) and O 1s (d) of Cu_2O NCs and after HA adsorption.

Photodegradation of organic pollutants from water

To demonstrate the photocatalytic activity of obtained Cu_2O NCs as a novel integrated photocatalytic adsorbent (IPCA), photodegradation experiments of organic pollutants (HA, CR, MO and TC) were carried out with visible light illumination after adsorption. Typically, total concentrations of HA were simply determined from the maximum absorption ($\lambda = 254$ nm) measurements by UV-Vis spectroscopy. C/C_0 was used to describe the degradation (C and C_0 are HA concentrations at time t and 0, respectively). On the basis of the above batch experiments, the suspensions were magnetically stirred in the dark for 30 min to establish adsorption/desorption equilibrium of HA on the catalysts. The comparison of in photocatalytic activity of as-prepared Cu_2O NCs, CM Cu_2O and P25 is shown in Fig. 5a. Cu_2O NCs display much higher adsorption, and better photocatalytic activity than CM Cu_2O and P25, and about 99.5% of HA molecules can be completely decomposed within 120 min. The inset photographs in Fig. 5a show the corresponding color changes of initial concentration solution of HA and supernatant liquid after photodegradation. To verify the stability and reusability of Cu_2O NCs, cycling experiments were tested to evaluate the decreased concentration of HA under the same reaction conditions during the cycling tests. As shown in Fig. 5b, the recovered Cu_2O NC sample for the degradation of HA exhibits a high activity and good recyclability as the conversion just a slight decline even after 5 cycling tests. More than 84% of the original HA was degraded, while the degradation efficiency is 99.5% for the 1st run, confirming that our Cu_2O NCs are stable visible-light photocatalysts. These results clearly demonstrate that our obtained Cu_2O NCs can be used as an efficient IPCA for the purification of contaminated water.

Furthermore, Cu_2O NCs can also photodegrade acidic/anionic dyes such as CR and MO. As shown in Fig. S8,† Cu_2O NCs degrade about 99% CR and 90% MO in 120 min, while CM Cu_2O shows a small amount of adsorption and ignorable degradation of each dye. From the degradation of CR and MO on Cu_2O NCs, the characteristic absorption band diminishes quickly under visible light irradiation (Fig. S8b and S8d†). The

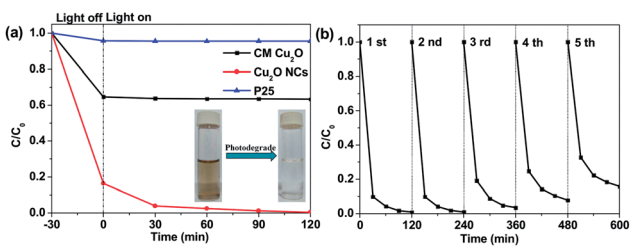

Fig. 5 Photodegradation of HA (a) over CM Cu_2O and obtained Cu_2O NCs under visible light irradiation ($\lambda \geq 400$ nm). The inset photographs are the initial solution of HA and the supernatant liquid after degradation. Cycling runs in the photodegradation (b) of HA in the presence of Cu_2O NCs under visible light irradiation.

inset photographs show the corresponding color changes of dyes solutions with the increasing reaction time (inset in Fig. S8a and S8c†). Pseudo-first-order kinetics reaction was applied to simulate the experimental data with the Langmuir–Hinshelwood model ($\ln(C_0/C) = kt$, where k is the pseudo-first-order rate constant, and was determined from a linear fit to the experimental data). Fig. S9† shows that the decomposition of HA, CR, and MO followed the pseudo-first-order model well. Moreover, Cu_2O NCs can degrade about 75% tetracycline molecules in 3 h (Fig. S10a†), and the pseudo-first-order model is also used for the photocatalytic degradation of TC (Fig. S10b†). In addition, we measured the total organic carbon (TOC) and the TOC removal curve is shown in Fig. S11 in the ESI,† from which it can be clearly observed that the HA can be thoroughly mineralized to CO_2 and H_2O, demonstrating the strong photooxidative ability of obtained Cu_2O NCs.

To investigate the optical response of the obtained samples, the UV-Vis absorption spectra of as-prepared Cu_2O NCs and CM Cu_2O samples are shown in Fig. 6a. It is evident that Cu_2O NCs display a blueshift in the optical absorption compared with CM Cu_2O. Compared with the UV-Vis diffuse reflectance spectra of Cu_2O NCs before and after HA adsorption, the absorbance of Cu_2O NCs–HA was enhanced, indicating that a little light absorption improvement increased photocatalytic activity (Fig. S12†). For our obtained Cu_2O NCs, the extrapolated value (a straight line to the x-axis) of E_{photon} at $\alpha = 0$ gives absorption edge energies corresponding to E_g that is the band gap of the material, which follows plots of $(\alpha E_{photon})^{1/2}$ *versus* the energy of absorbed light (where α and E_{photon} are the absorption coefficient and the discrete photon energy, respectively). Fig. 6b shows that the samples have optical absorption gaps of 2.03 eV and 1.98 eV for Cu_2O NCs and CM Cu_2O, respectively. A little larger band gap is observed for Cu_2O NCs, as compared to that of CM Cu_2O at 1.98 eV, which is attributed to the quantum size effect, in consistent with blue shift of the adsorption edge presented in Fig. 6a.[26] The valence band XPS spectra (VB-XPS) near the Fermi level were provided to explore the electronic structure of the as-prepared samples. The valence band maximum (VBM) edge potentials of cuprous ion were measured by the VB-XPS spectra to demonstrate the band alignment occurred for CM Cu_2O and Cu_2O NCs. As shown in Fig. 6c, the VBM energy levels of Cu_2O NCs and CM Cu_2O were determined to be about 0.51 eV and 0.47 eV, indicating that the VBM position of Cu_2O NCs shifted toward high binding energy. Combined with the UV-Vis data above, the conduction band minimum (CBM) changed slightly (from −1.51 to −1.52 eV) by computation. Herein, the higher binding energy of VBM made the valance band potential more positive, which may evidently enhance the redox capacity and photocatalytic activity. The wider band gap is closely related to a smaller size of obtained Cu_2O NCs, generating from the quantum size effect. Hence, the energy gap of the semiconductor broadens, oxidation–reduction potential enlarges and photocatalytic reaction driving force increases, leading to improved photocatalytic activity due to the quantum size effect.[27] The integrated adsorption and photocatalysis degradation mechanism of HA over Cu_2O NCs is proposed in Scheme 1. First, HA adsorption occurs mainly through surface complexation as well as coagulation on the surface of Cu_2O NCs. Then, during the process of the semiconductor-initiated photocatalytic reaction, Cu_2O NCs can create electron–hole (e^-/h^+) pairs upon visible light excitation. The photogenerated electrons on the surface of Cu_2O NCs may react with O_2 and H_2O to generate $\cdot O_2^-$, $\cdot OH$ radicals and other reactive oxygen species. The hydroxyl groups form $\cdot OH$ radicals by trapping photogenerated holes (h^+). The $\cdot OH$ radicals are well known as a very strong oxidant to degrade organic pollutants owing to their high oxidizing potential (2.8 V).

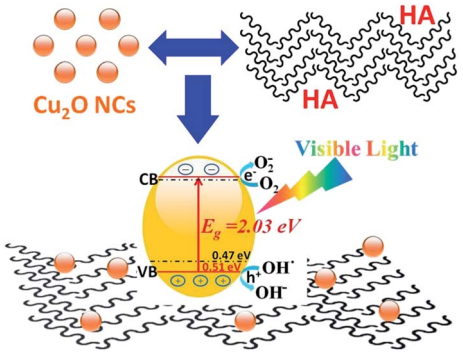

Scheme 1 Schematic integrated adsorption and degradation of HA over Cu_2O NCs under visible-light illumination.

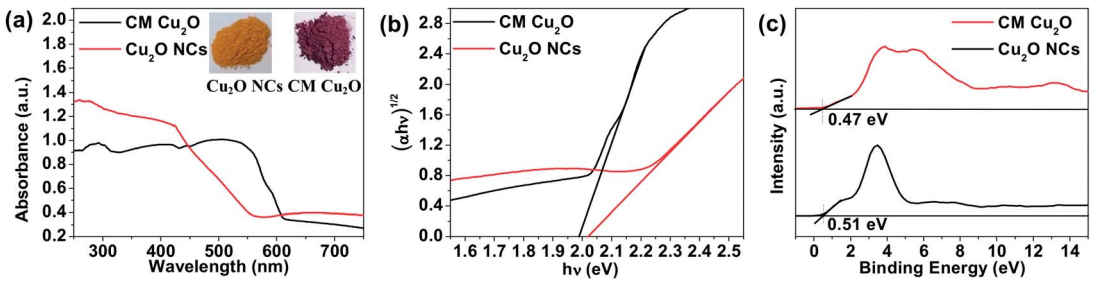

Fig. 6 The UV-Vis diffuse reflectance spectra (a) and band-gap evaluation (b) from the plots of $(\alpha E_{photon})^{1/2}$ *vs.* the energy of the absorbed light of the CM Cu_2O and Cu_2O NCs. The insets in (a) are the corresponding photographs. The VB-XPS spectra (c) of as-prepared Cu_2O NCs and CM Cu_2O.

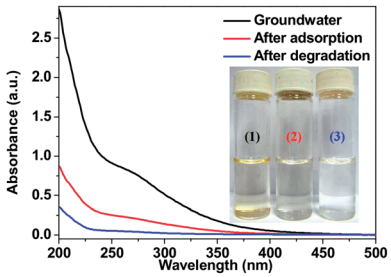

Fig. 7 The UV-Vis spectra of the natural groundwater sample (vial 1), after adsorption treatment in the dark for 30 min (vial 2), and then photodegradation by visible light for 120 min (vial 3).

Natural wastewater treatment using Cu_2O NCs as an integrated photocatalytic adsorbent (IPCA)

Based on the above experiment results, the as-synthesized Cu_2O NCs were used for purification of real wastewater. Natural groundwater sample was pumped out from a groundwater well (from Xing-Wang Village in Togtoh County, Inner Mongolia Autonomous Region, China), which provides drinking water for local residents (Fig. S13a and S13b†).[28] As can be seen from Fig. S13c and S13d,† the strongest fluorescence position at the excitation and emission wavelength at 280 nm and 420 nm is displayed in excitation emission matrix fluorescence spectroscopy and the molecular weight of natural organic matter (NOM) is centered at 3000 Da (peak 1) and 1500 Da (peak 2), indicating that the main species of NOM in the groundwater sample are humic acid substances. In this study, the groundwater containing HA was tested on our as-prepared Cu_2O NCs as IPCA. The UV-Vis absorbance spectra of the natural groundwater, after adsorption and afterward degradation are shown in Fig. 7. The adsorption of HA on Cu_2O NCs reached saturation after approximately 30 min in the dark, during which the UV_{254} absorption intensity declined from 0.885 to 0.245. And then, under visible light irradiation for 2 h, more than 94% of NOM was removed by Cu_2O NCs, suggesting that Cu_2O NCs, displaying high adsorption capacity combined with efficient photocatalytic degradation, are favorable for the application of deep purification of contaminated drinking water.

Conclusions

In conclusion, Cu_2O NCs as a new IPCA have been prepared by a synproportionation reaction of Cu^{2+} and copper metal at room temperature. The Cu_2O NCs with a uniform size display excellent adsorption affinity and superior photocatalytic degradation of organic pollutants from aqueous systems. The maximum adsorption capacity toward HA reaches 405.5 mg g^{-1}, furthermore, about 99.5% of HA molecules can be completely decomposed within 120 min with visible light irradiation. More importantly, the Cu_2O NCs display a remarkable integrated adsorption photocatalytic performance for other organic pollutants in water, such as CR, MO and TC. Based on SEM, TEM, VB-XPS, and UV-Vis absorbance results, the excellent pollutant purification can be ascribed to the smaller particle size, high specific surface area and the quantum size effect. Moreover, the reusability of Cu_2O as IPCA has also been confirmed. More than 94% of NOM was removed from drinking water by Cu_2O NCs in the Inner Mongolian area, demonstrating that our obtained Cu_2O NCs can be used as a suitable IPCA material for effective decontamination of natural ground water.

Acknowledgements

The authors acknowledge financial support from the National Basic Research Program of China (2011CB933700 and 2010CB934700) and the National Natural Science Foundation of China (21271165).

Notes and references

1 M. Petrovic, M. Gros and D. Barcelo, *J. Chromatogr. A*, 2006, **1124**, 68–81.
2 M. Klavarioti, D. Mantzavinos and D. Kassinos, *Environ. Int.*, 2009, **35**, 402–417.
3 C. J. Volk and M. W. LeChevallier, *J. - Am. Water Works Assoc.*, 2002, **94**, 112–123.
4 S. D. Richardson, in *Encyclopedia of Environmental Analysis and Remediation*, ed. R. A. Meyers, Wiley, New York, 1998, pp. 1398–1421.
5 J. Li, X. Xiao, X. Xu, J. Lin, Y. Huang, Y. Xue, P. Jin, J. Zou and C. Tang, *Sci. Rep.*, 2003, 3.
6 P. Zuman and J. Ludvík, *Electroanalysis*, 2000, **12**, 879–888.
7 T. Thorsen, *Water Sci. Technol.*, 1999, **40**, 105–112.
8 X. Lu, Z. Chen and X. Yang, *Water Res.*, 1999, **33**, 3271–3280.
9 S. P. Yang, O. Bar-Ilan, R. E. Peterson, W. Heideman, R. J. Hamers and J. A. Pedersen, *Environ. Sci. Technol.*, 2013, **47**, 4718–4725.
10 C. P. Chen, P. Gunawan and R. Xu, *J. Mater. Chem.*, 2011, **2**, 1218–1225.
11 S. Basha, C. Barr, D. Keane, K. Nolan, A. Morrissey, M. Oelgemöller and J. M. Tobin, *Photochem. Photobiol. Sci.*, 2011, **10**, 1014–1022.
12 V. Vimonses, B. Jin, C. W. K. Chow and C. Saint, *Water Res.*, 2010, **44**, 5385–5397.
13 J. C. Crittenden, R. P. S. Suri, D. L. Perram and D. W. Hand, *Water Res.*, 1997, **31**, 411.
14 C. M. Fan, Y. Peng, Q. Zhu, L. Lin, R. X. Wang and A. W. Xu, *J. Phys. Chem. C*, 2003, **117**, 24157–24166.
15 Y. Zhang, B. Deng, T. Zhang, D. Gao and A. W. Xu, *J. Phys. Chem. C*, 2010, **114**, 5073–5079.
16 K. Borgohain, N. Murase and S. Mahamuni, *J. Appl. Phys.*, 2002, **92**, 1292–1297.
17 V. Ischenko, S. Polarz, D. Grote, V. Stavarache, K. Fink and M. Driess, *Adv. Funct. Mater.*, 2005, **15**, 1945–1954.
18 N. Zhang, R. Yi, R. Shi, G. Gao, G. Chen and X. Liu, *Mater. Lett.*, 2009, **63**, 496–499.
19 D. H. Wang, L. Jia, X. L. Wu, L. Q. Lu and A. W. Xu, *Nanoscale*, 2012, **4**, 576–584.
20 T. Wen, X. L. Wu, X. L. Tan, X. K. Wang and A. W. Xu, *ACS Appl. Mater. Interfaces*, 2013, **5**, 3304–3311.

21 S. V. Prasanna and P. V. Kamath, *J. Colloid Interface Sci.*, 2009, **331**, 439–445.
22 C. Forano, *Interface Sci. Technol.*, 2004, **1**, 425–458.
23 J. M. Gong, T. Liu, X. Q. Wang, X. L. Hu and L. Z. Zhang, *Environ. Sci. Technol.*, 2011, **45**, 6181–6187.
24 X. Y. Yu, T. Luo, Y. Jia, R. X. Xu, C. Gao, Y. X. Zhang, J. H. Liu and X. J. Huang, *Nanoscale*, 2012, **4**, 3466–3474.
25 F. Liu, Y. J. Jin, H. B. Liao, L. Cai, M. P. Tong and Y. L. Hou, *J. Mater. Chem. A*, 2013, **1**, 805–813.
26 C. H. Kuo, C. H. Chen and M. H. Huang, *Adv. Funct. Mater.*, 2007, **17**, 3773–3780.
27 W. K. Leutwyler, S. L. Bürgi and H. B. Burgl, *Science*, 1996, **271**, 933–937.
28 X. L. Wu, X. L. Tan, S. B. Yang, T. Wen, H. L. Guo, X. K. Wang and A. W. Xu, *Water Res.*, 2013, **47**, 4159–4168.